[1]**Manoj Kumar**

[2]**Manish Patidar**

[3]**Narendra Singh**

Filtered Ofdm System Model for Papr Reduction in the Growth Of 5g

JES

Journal of Electrical Systems

Abstract: - A proposed waveform for fifth generation (5G) communications is the filtered orthogonal frequency division multiplexing (F-OFDM) system. Filtering-based waveform frameworks distinguish themselves by suppressing out-of-band emission and asynchronous transmission. Meanwhile, the high Peak-To-Average Power Ratio (PAPR) remains a barrier to new waveform possibilities. Partials transmit sequence (PTS) is a successful strategy for reducing high PAPR in multicarrier networks. This work presents a multicarrier in OFDM and UFMC based on the Filter Bank Multicarrier (FBMC) waveform for communication systems. Furthermore, FBMC waveforms have limited orthogonality between subcarriers, which can mitigate Doppler and multipath effects. This FBMC approach uses the cosine law to filter the traffic signal, and the Welch algorithm is offered for segmentation, which lowers noise in estimated power spectra. As a result, a hybrid Selective Mapping (SLM) with Cuckoo Search and Ant Lion Optimization (CS-ALO) algorithms is suggested using the FBMC framework to reduce PAPR in the OFDM system. The proposed work is implemented, and detailed experimental research is carried out to show the increased performance in 5G networks. Based on a fair comparison, the F-OFDM scheme outperforms previous approaches in terms of BER and multicarrier system capacity. Simulation results show that the proposed waveform design and processing method outperform standard OFDM and F-OFDM methods in PAPR reduction and communication integrated systems.

Keywords: Filtered orthogonal frequency division multiplexing, 5G Network, filter bank multicarrier, Guard Interval Sequence Selection, PAPR Reduction, and Multicarrier Modulation System.

I.   INTRODUCTION

The annual surge in data traffic within communication systems is accelerating at an unprecedented pace, propelling the imminent need for a nearly 1000-fold increase in capacity. The forthcoming era of 5G is poised as a potential savior, promising throughput in the realm of multiple gigabits per second to satiate this incessantly burgeoning demand [1]. Beyond merely quenching the thirst for higher data rates, 5G technology is envisioned to fortify reliable transmission and reception for the expanding array of devices tethered to networks. Moreover, it stands as a catalyst for advancing nascent technologies such as smart urban environments, immersive virtual experiences, and the interconnected realm of intelligent transportation.

systems. To meet the escalating need for elevated data speeds spurred by cutting-edge technologies, 5G is a pivotal player. Given its remarkable spectral efficiency and resilience in complex multipath environments, OFDM has become a cornerstone in modern communication systems. The fusion of MIMO with OFDM heralds a developing expertise for high-speed data multi-carrier transmission, finding applications in 4G and 5G mobile networks, medical body area networks, and digital audio-video broadcasting [2].

A prevalent challenge in multicarrier transmissions, particularly impacting OFDM, is the issue of high PAPR. This phenomenon, resulting from coherent coincidences of carrier phases and frequencies, leads to significant increases in instantaneous power outputs surpassing the mean power of the high-power amplifier (HPA).

[1]Department of Electronics and Communication Engineering, Jaypee University of Engineering and Technology,

Guna, India.

manoj1985.111@gmail.com

2Department of Electronics and Communication Engineering, Jaypee University of Engineering and Technology,

Guna, India.

manish.patidar@juet.ac.in

3Department of Electronics and Communication Engineering, Jaypee University of Engineering and Technology,

Guna, India.

narendra.singh@juet.ac.in

Extensive research efforts have delved into addressing this PAPR problem [3][4]. OFDM employs three key methods for data transmission: i) multiple carriers, referred to as subcarriers, for data streams; ii) orthogonal alignment of subcarriers; and iii) insertion of a CP to ease ISI as well as reduce channel delay spread [5][6].

To scrutinize the waveform behavior modulation concerning PAPR in the 5G system, an ongoing experiment is underway [7]. Evaluation metrics encompass BER and FER. The investigation consistently underscores the outperformance of FBMC over f-OFDM expressed in the context of BER and FER. Marked performance degradation in the f-OFDM scheme, attributed to its substantial PAPR, has prompted the recommendation of an effective PAPR-reduction technique. The proposed two-piecewise compounding (TPWC) technique, discerningly assessing large and small amplitudes separately, adeptly minimizes peak power, showcasing both piecewise linear and continuous properties [8].

The nonlinear segment of the HPA grapples with OFDM signal alteration owed to elevated PAPR, leading to a consequent decrease in BER. An immensely appealing avenue for PAPR reduction is the PTS method. However, the conventional PTS technique is plagued by computational complexity and high costs, necessitating a crucial enhancement in computational efficiency to optimize PTS conditions for effective PAPR reduction [9]. Introducing an alternative multicarrier modulation approach for 5G wireless networks, the UFMC system exhibits promise. The UFMC system holds potential advantages such as increased spectrum efficiency, robustness, reduced latency, and diminished out-of-band emission. Nevertheless, the UFMC system grapples with a substantial challenge in the form of high PAPR, severely impacting the high-peak signal through the HPA [10].

Envisioning the evolution of the 5G network, there is an anticipation of heightened system capacity, robust connectivity, and the ability to handle millions of devices at unprecedented speeds [11][12]. In the realm of 5G and subsequent wireless communications, F-OFDM stands out as one of the most prominent Multicarrier Modulation (MCM) algorithms [13,14]. However, the pervasive PAPR issue associated with F-OFDM elevates the risks of signal distortion and compromises the efficiency of Power Amplifiers (PA). A judicious hybrid PAPR reduction solution is imperative; amalgamating the proven classical SLM with the iterative Clipping and Filtering (ICF) approaches to address elevated PAPR challenge in F-OFDM outlines [15].

This study undertakes a hybrid optimization technique to alleviate the elevated PAPR value in the F-OFDM classification of OFDM grounded on the hybrid optimization method. OFDM finds extensive use in contemporary multimedia communication schemes; the frequency band undergoes segmentation in numerous compact narrowband conduits. Yet, a notable drawback arises from the excessive amplitude of the time-domain signal in OFDM, pushing it towards nonlinear amplification. This scenario poses a myriad of challenges that adversely affect the overall framework performance, making capability analysis imperative for effective resource management in the OFDM system [16].

A key focus of this research revolves around the need to overcome the PAPR of conventional OFDM signals and those created using traditional techniques. The research endeavors to explore and put forward strategies that are both operative and effectual in mitigating PAPR in OFDM based setups. These proposed techniques are designed to harmonize with practical considerations and find tangible applications in real-world scenarios [17]-[19].

II. PROPOSED RESEARCH METHODOLOGY

The burgeoning demand for innovative wireless services, coupled with the existing spectrum shortage challenge, has propelled the exponential growth in wireless communication. To address this, a 5G-MIMO grounded Cognitive Radio (CR) communication setup was devised, aiming for augmenting the spectrum utilization through the implementation of a Spectrum Sensing (SS) algorithm. The proposed SS algo relies on the Hybrid Filter Detection (HFD) procedure to enhance spectrum efficiency. In the realm of 5G wireless networks, essential requisites include high data rates, minimal power consumption, and exceedingly low end-to-end latency. Consequently, there is a pressing need for continuous advancements in the design and performance of 5G physical layer waveforms. The conventional OFDM faces a notable drawback in the form of PAPR, leading to signal distortion and a subsequent reduction in system efficiency. Considering this, the primary objective of this study is to assess multicarrier systems, particularly focusing on OFDM and UFMC systems, and their applicability to 5G wireless networks. The proposed work's process block diagram is illustrated in Figure 1, providing an overview of the envisaged study. Through this investigation, the study aims to contribute insights into the efficacy of these multicarrier systems in meeting the evolving demands of 5G wireless networks.
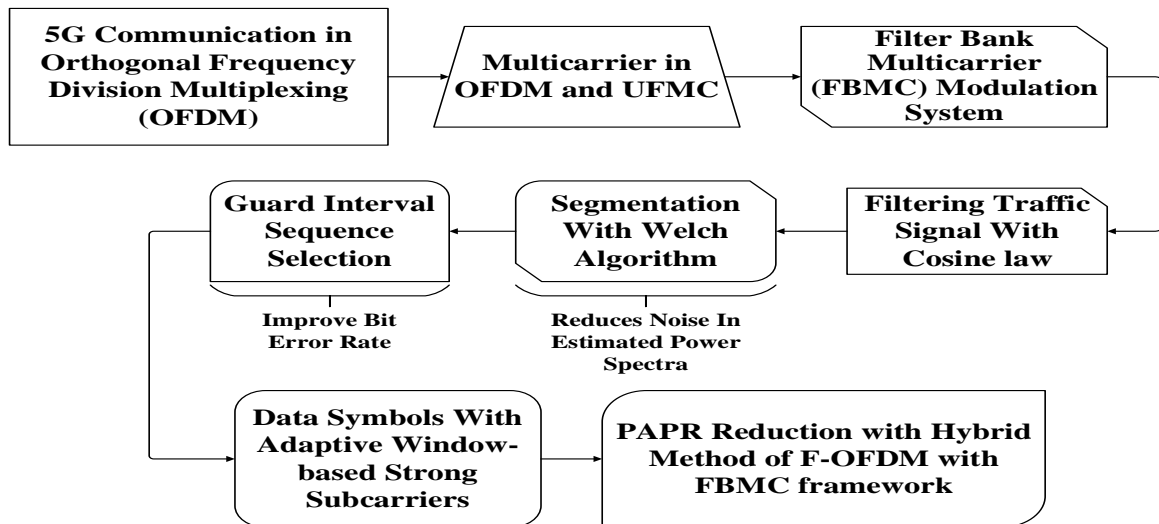
Figure 1. Illustration of the Introduced Work

FBMC emerges as a potent modulation technique poised to play a pivotal role in future 5G wireless networks, particularly over massive mMIMO channels. Distinguishing itself from the widely utilized OFDM technique, FBMC stands out for its efficacy in providing high spectral efficiency while demonstrating resilience against synchronization errors. The FBMC modulation scheme operates as a multi-carrier setup with an extensive dynamic range. Its fundamental purpose revolves around enhancing the spectral qualities of the conveyed signal. Key element of this scheme is the filter, which plays a critical part in determining the signal characteristics. Employing the Cosine law for filtering the traffic signal, FBMC achieves modulation by modulating the pulse of the filter. This intricate process is further refined by the application of the Welch algorithm, facilitating segmentation.

III.   UNIVERSAL FILTER MULTI CARRIER (UFMC)

UFMC meticulously sieves each sub-band, comprising orthogonal multi-carriers, to effectively diminish Out-of-Band (OOB) power [6]. RF chain transforms the acknowledged signal into a baseband signal. Subsequently, an Analog-to-Digital Converter (ADC) alters the baseband signal into a digital signal. Following this, time-domain pre-processing takes place. Upon completion of the procedure, a series data stream undergoes transformation into a parallel data stream through a Serial-to-Parallel (S/P) conversion. The time-domain parallel data stream is further transformed into a frequency-domain stream through a 2N-FFT operation [20]-[22]. Following the 2N-FFT procedure, the data symbols with odd-numbered indices are specifically selected and subjected to equalization [23] [24].

IV.   FILTER BANK MULTI CARRIER (FBMC)

Within the FBMC system's transmitter, data symbols undergo a transformation from a series stream to a parallel stream through Serial-to-Parallel (S/P) conversion. Parallel symbols undergo modulation, resulting in the creation of an OQAM signal [25]. The OQAM signal, enriched by modulation, undergoes a subsequent metamorphosis in a meticulously crafted waveform, elegantly sieved by each sub-carrier. This intricate process unfolds within the confines of a sophisticated synthesis filter bank, harmoniously combining the prowess of an IFFT and a PPN (Polyphase Network). Ultimately, the magnified FBMC signal gracefully embarks on its journey through the antenna, propelled into the ether. The recipient on the FBMC setup gracefully unveils a configuration mirrored in contrast to the FBMC transmitter, completing the symphony of signal transmission and reception [26]-[30].

4. UFMC-FBMC System Model

The UFMC system represents a generalized version of OFDM, departing from the use of a CP. It divides the assigned bandwidth into distinct sub-bands, employing finite impulse response (FIR) filtering on each sub-band before transmission. This filtering effectively mitigates spectral side-lobe levels, enhancing robustness. In contrast to OFDM, the Filtered FBMC system transmits offset QAM symbols, where the tangible and abstract facets of intricate Quadrature Amplitude Modulation (QAM) representations undergo a meticulous separation. Following

this, each distinct facet is meticulously conveyed with a precise half-symbol period displacement during the transmission phase. Diagram 1 illustrates FBMC system, executed through a filter bank and IFFT. The transmitted symbol's o/put via the synthesis filter bank (SFB) is expressed in eq. (1).

$$s(l) = \underbrace{\sum_{m=0}^{M-1} \sum_n a_{m,n} g\left(1 - n\frac{M}{2}\right) e^{j2\pi ml/M} e^{j\varphi_{m,n}}}_{g_{m,n}(l)} \tag{1}$$

Where, M depicts subcarrier no., $a_{m,n}$ is actual data on the mth subcarrier of the nth FBMC symbol, and phase factor $\varphi_{m,n}$ is set to $(\frac{\pi}{2})(m+n)$. $g(l)$ signifies the prototype filter with dimension $L_g = KM$, here, K symbolizes the overlap factor $g_{m,n}(l)$ embodies the synthesis basis gained from the TF alteration of $g(l)$ Following the channel and analysis filter bank (AFB), the demodulation symbol at TF point (p, q) is given in eq. (2).

$$y_{p,q} = \sum_{m=0}^{M-1} \sum_n a_{m,n} \sum_l g_{m,n}(l) g *_{p,q}(l), \tag{2}$$

Here, the orthogonality criterion of g(l) is met, ensuring the conditions for flawless signal rebuilding satisfies $\Re\{\sum_l g_{m,n}(l) g *_{p,q}(l)\} = \delta_{m,p} \delta_{m,p}. \delta_{m,q}$ designates the Kronecker delta function viz equal to 1 if $m = p$ and corresponds to 0 if $m \neq p$. Consequently, the FBMC receiver can precisely recover the transmitted symbol by extracting the actual chunk of the demodulated symbol. In the case of F-OFDM, the filtering operation typically involves hybrid filter detection. This process begins with an evaluation of noise in data traffic, followed by reducing variance in noise. The consequent phase involves eliminating null coefficients associated with R[k], thereby reducing sensing temporal and computational requirements. Thus, K' is the restructured $R[k]$ length, here K' < K (i.e., $R'[k]$ is the $R[k]$ with K' length). To capture the nuances of traffic dynamics, a considerable number of trials are essential. The deployment of a cosine filter was executed, wherein R' [k] underwent segmentation into Nseg segments. Each segment, characterized by a length of Lseg, was assessed through the Welch segmentation tactic. Subsequently, the removal of null coefficients from all segments ensued, streamlining the overall complexity of the process.

$$R_{F-MIMO-OFDM}[K] = (-1)^k \sum_{v=0}^{V-1} \sum_{b=0}^{B-1} \sum_{m=0}^{M-1} \sum_{l=o}^{L-1} \sum_{n=0}^{N-1} \times \frac{s_{m,n}^b g_b[l] e^{j2\pi \frac{(nR-1-mc)}{N}}}{\sqrt{V}} +$$

$$\sqrt{\frac{2}{V}} \sum_{v=0}^{V-1} \sum_{b=0}^{B-1} \sum_{m=0}^{M-1} \sum_{l=o}^{L-1} \sum_{n=0}^{N-1} s_{m,n}^b g_b[l] e^{j2\pi \frac{(n-1-mC)}{N}} cos\left(\frac{\pi kR(2v+1)}{2V}\right), 0 \leq k \leq K-1 \tag{3}$$

$$R[k] = \frac{2}{v} \sum_{v=0}^{V-1} r[v] cos\left(\frac{\pi kR(2v+1)}{2V}\right), 1 \leq k \leq K-1 \tag{4}$$

The proposed hybrid technique demonstrates lower computational complexity, making it a favorable choice for reduced runtime. This approach achieves a significant reduction in computational complexity, focusing on mean operations and real values. The Bartlett Welch method divides the signal into smaller segments, computes averages, and simplifies arithmetic operations. With straightforward additions and rate calculations, the method involves no integrals, differentials, or natural logarithms. This simplicity, dealing only with real numbers, contributes to the overall reduction in complexity. The MIMO (F-OFDM) waveforms benefit from this hybrid filter approach, emphasizing simplicity in implementation [27]-[30].

V.   PAPR ON F-OFDM

 The elevated PAPR is deemed a notable vulnerability in the practical implementation of multi-carrier systems rooted in Orthogonal Frequency Division Multiplexing (OFDM), recognized for its inherent orthogonality in transmission. It is characterized as the highest ratio of the signal-transmitted peak power to the mean signal power. F-OFDM stands out as a candidate for 5G waveforms, introducing a paradigm of sender and receiver strainers across the frequency spectrum. The F-OFDM signal is attained by conveying the OFDM signal denoted as z(n) through a useful spectrum-shaping filter represented by g(n).

$$K(n) = z(n) * g(n) \tag{5}$$

Where, g(n) represents the finite impulse response coefficient of a transmitter filter. Crafted with a length O, precisely equivalent to the average length of the OFDM symbol plus one, the filter is meticulously designed to

embody both adaptability and filtration efficiency. Subsequently, the received signal undergoes traversal through the receiver filter denoted as g*(-n).

$$\overset{\frown}{k}(n) = z(n) * g(n) * g(-n) \tag{6}$$

In this context, g*(-n) symbolizes the finite section of the impulse response of the transmitter filter, aligning with the transmit filter. The Sinc pattern in the time domain is thus articulated, as conveyed in the ensuing equations.

$$g(n) = hLPF(n) * Wrrc(n) \tag{7}$$

$$h_{LPF}(n) = \frac{\sin(w_c * n)}{w_c * n} \tag{8}$$

$$W_{RRC}(n) = \left[0.5 \left(1 + cos \left(\frac{2\pi n}{o-1} \right) \right) \right]^r \tag{9}$$

Where, $h_{LPF}(n)$ depicts LPF impulse response, $W_{RRC}(n)$ signifies impulse response of a window mask, w_c denotes LPF trimmed-off frequency, whereas r expresses roll-off factor monitoring the shape of the window. RRC window roll-off factor is limited to $0 < r < 1$, giving supplementary flexibility to deliver a respectable equilibrium between the frequency and timing position.

VI. SELECTIVE MAPPING WITH CUCKOO SEARCH

Algorithm

The SLM-CS methodology finds applicability within both the OFDM and F-OFDM frameworks, effectively mitigating computational complexity while bolstering PAPR reduction efficiency. This amalgamated approach involves intricate manipulations of the transmitter across both the temporal and spectral domains within the OFDM or F-OFDM system. Furthermore, optimal phase factor indices for each segment of this collaborative process are transmitted to the recipient (SI) to facilitate the faithful reconstruction of the original information. The transmission procedures initiate with the origination of QAM symbols derived from the data bits. Post-modulation, these QAM symbols undergo segmentation into clusters corresponding to distinct sub-bands, with each related symbol cluster selectively allocated to its designated sub-band.

$$X_b(k) = \begin{cases} \lambda(k), if (b-1) \le k \le b \left(\frac{N}{B} \right) - 1 \\ 0, otherwise \end{cases} \tag{10}$$

Here, $K = 0,1,2,....,N-1; b = 0,1,2,....,B$, the sequence of QAM symbol is achieved in QAM modulator o/put which is expressed through $X(k)$, the frequency domain info is promoted to subband b, represented as $X_b(k)$, B signifies subband tally, k epitomizes subcarrier index and N directs subcarrier count. Nourishing the deployment of symbol groups to B subbands, IFFT is employed to all subbands as given in eq. (11).

$$X_b(N) = \frac{1}{\sqrt{N}} \sum_{k=0}^{N-1} \lambda_b(k) e^{\frac{j2\pi kn}{N}} \tag{11}$$

Where,$0 \le n \le N-1; 1 \le b \le B$, $X_b(n)$ symbolizes signal accomplished by altering $X_b(k)$ in the frequency to the time domain by IFFT block in the sub-band b. Upon the completion of IFFT operations within each sub-band, the resultant time-domain signal undergoes both CP addition and corresponding filtering procedures. Ultimately, the signal is derived from the output of a finite impulse response filter, a crucial component contributing to the formulation of the UFMC broadcast signal. The summation and filtration processes applied to time-domain sub-band signals are equated by eq. (12).

$$s(n) = \sum_{b=1}^{B} X_b(n) . f_b(n), 0 \le n \le N + L_{CP} + L_f - 1 \tag{12}$$

Impulse response pertains to the bth filter characterized by $f_b(n)$. Lf signifies strainer extent and LCP directs CP length. Furthermore, the PAPR of the broadcast signal is expressed as

$$PARP(dB) = 10 log_{10} \frac{0<n<N+L_{CP}+L_f |s(n)|^2}{E[|s(n)|^2]} \tag{13}$$

Hence, it is feasible to utilize the oppositional hosted cuckoo optimization (OHOCO) algo for the PAPR mitigation issue also incorporating it into the stage optimization job. Additionally, it's necessary to interpret 'zero' & 'one' in the resolution space of the OHOCO prototypical as (-1, 1) respectively.

6.1 Cuckoo Search Algorithmic Design

The COA algorithm is devised to address PAPR reduction in UFMC models. In this context, these avian species have the capacity to deposit their eggs within the nests of fellow bird species. The cuckoo adeptly mimics both the shape as well as egg coloration of the host's nest, with pivotal decisions made during the nesting process falling into three main modules. The crux of this practice can be encapsulated in the following summary.

Stage 1: Commence variable initialization. This phase entails introducing the upper limit for cuckoo generations N_{gen} additionally, the quantity M, denoting the number of nests, is considered as the habitat.

Stage 2: Generate the nesting structure. The creation of the nest unfolds following,

$$\begin{cases} Nest_1(r,n) = (r_1, r_2, \ldots, r_{m,} n_l, n_2, \ldots, n_m) \\ Nest_2(r,n) = (r_1, r_2, \ldots, r_{m,} n_l, n_2, \ldots, n_m) \\ Nest_M(r,n) = (r_1, r_2, \ldots, r_{m,} n_l, n_2, \ldots, n_m) \end{cases}$$

Here, Nest (n,r) symbolizes a collection of meaningful resolutions.

Stage 3: Compute the model's consistency and regulate constraints $R_s(r,n)$. The constraints are governed by the subsequent penalty function:

$$\overline{R}_s(r,n) = R_s(r,n) + \Phi_1.Max\{0, g_l(r,n) - V\} + \Phi_2.Max\{0, g_2(r,n) - \quad C\} + \quad \Phi_3.Max\{0, g_3(r,n) - W\}$$
(14)

Stage 4: Cuckoo eggs are deposited utilizing the HOCO algorithm.

$$ELR = \alpha + \frac{Number\ of\ current\ cuckoo's eggs}{Total\ number\ of\ eggs} \times (V_{hi} - V_{low})$$ (15)

Where ELR denotes laying radius, α designates integer value, V_{hi} together with V_{low} Signifying the upper and lower limits of the parameters respectively, the range of eggs a cuckoo may lay is assumed to vary between two and four.

$$\begin{cases} M_1 nests\ with \sigma_1, where\ M_1 \epsilon\{M\} \\ M_2 nests\ with \sigma_2, where\ M_2 \epsilon\{M - M_1\} \\ M_3 nests\ with \sigma_3, where\ M_3 \epsilon\{M - M_2 - M_1\} \end{cases}$$ (16)

Stage 5: During the migration phase, the optimal generation of cuckoos migrates to other habitats, housing the optimal resolutions. These resolutions can subsequently be introduced in the following generation to enhance the search for resolutions.

Stage 6: Iterate through steps 2 to 6 until Ngen is achieved. To enhance the convergence rate of the SLM-CS model, infuse the ALO concept into the devised algorithm.

6.2 Ant Lion Optimization (ALO) Algorithm

The ALO algorithm, known for its extended runtime, is addressed, and optimized through random walkways innovation. The PL-ALO algorithm exhibits faster performance than the original ALO method in certain test functions. In this algorithm, ants shift towards the antlion at a specified slippage rate. Notably, the existing ALO model considers only a threshold greater than 0.5, leading to potential solution losses and reduced investigation. The PL-ALO prototypical introduces a divider possibility with IV thresholds, enhancing examination. In PL-

ALO, the process of tossing sand is utilized for shifting ants as well as the antlion's pit, as expressed in equations (17-18).

$$C_i^t = \begin{cases} Antlion_i^t + C^t, & for\ 0.75 < option < 1 \\ Antlion_i^t - C^t, & for\ 0.5 < option < 0.75 \\ -Antlion_i^t + C^t, & for\ 0.25 < option < 0.5 \\ -Antlion_i^t - C^t, & for\ option < 0.25 \end{cases} \quad (17)$$

$$d_i^t = \begin{cases} Antlion_i^t + d^t, & for\ 0.75 < option < 1 \\ Antlion_i^t - d^t, & for\ 0.5 < option < 0.75 \\ -Antlion_i^t + d^t, & for\ 0.25 < option < 0.5 \\ -Antlion_i^t - d^t, & for\ option < 0.25 \end{cases} \quad (18)$$

Within this refined model, the randomly selected variable assumes a pivotal role in updating shift rates through expedited hunting mechanisms & conditions, culminating in a more precise and effective mechanism. This enhancement leads to more precise results in redirecting the search space of ants. Unlike the original ALO method, where the best antlion is updated at the end of each iteration, this model combines ant and antlion populations. These populations undergo ranking based on their fitness standards, and half of the amalgamated population is designated as the antlion location for the ensuing repetition. The enhancement in the selection method encompasses a comparison of each ant-antlion pair with the antlion's fitness value, leading to cataloguing and population amalgamation. If an ant's fitness value surpasses that of the antlion, the ant's position is then adopted as the revised antlion position, delineated in equation (19).

$$Antlion_i^t = Ant_i^t\ iff\ (Ant_i^t) < f(Antlion_i^t) \quad (19)$$

Here the position of the antlion is depicted as $Antlion_i^t$, t is repetition, i is antlion, antlion fitness $f(Antlion_i^t)$, the fitness of ants illustrated with the help of $f\ Ant_i^t$, and the position of the ant expressed through Ant_i^t. The populace in this algo primarily resides at identical boundary points for most quest agents. In the context of ALO, a novel procedure is employed in lieu of the boundary technique. This alteration enhances the exploration performance within the ALO method. Ants are randomly deployed in the search space according to the mathematical prototypical, as delineated in equation (20).

$$Ant_i^t = b_{low} + rand \times (b_{up} - b_{low})\ if\ Ant_i^t > b_{up}\ or\ Ant_i^t < b_{low} \quad (20)$$

In this context, the random number within the interval is represented as $rand$, where the lower frontier is extended, and the upper frontier of the search space is denoted as b_{up}. The roulette wheel scheme is enlisted for each ant to navigate around an antlion.

The optimization method enhances the superiority of the prepared populace resolution by expanding it. The ALO tactic functions by exploring both orders of the exploration space, comprising of original and conflicting resolutions. Finally, the CS-ALO tactic selects the most suitable resolution from both directions, choosing the one with the lowest peak power. This further contributes to dropping the PAPR in OFDM setup.

VII.   7. RESULTS DISCUSSION

Embarking on this segment, a thorough comparative analysis unfolds between OFDM and F-OFDM waveforms. The scrutiny extends to both instances, encompassing the presence or absence of PTS techniques. The focal points of this investigation lie in assessing the presentation regarding PAPR, frequency localization, BER, and assessing intricacy. The simulation constraints are meticulously configured, with N established at 256 and 512, U set at 4, a constant M at 4, and a specified amount of stage influences (R) standing at 4. For F-OFDM, an LPF & RRC windowing mask with a roll-off feature of 0.6 is employed. The evaluation of PAPR utilizes the CCDF function, considering 1000 sub-frames for both OFDM and F-OFDM. Additionally, 64-QAM and 16-PSK are chosen for constellation mapping.
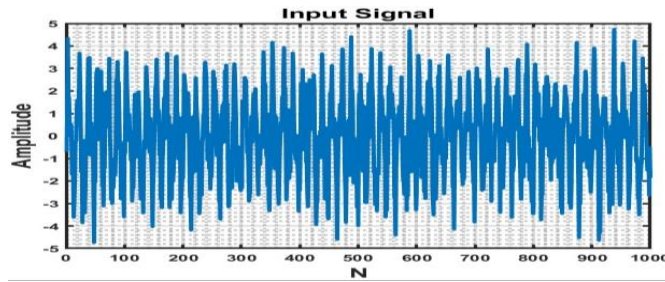
Figure 2. Amplitude Dispersal of traditional OFDM Signals

Figure 2 illustrates the amplitude dispersal of the clipped signal for a substantial number of subcarriers. The figure demonstrates that the clipped signals are consistently dispersed, which effectively reduces the PAPR.
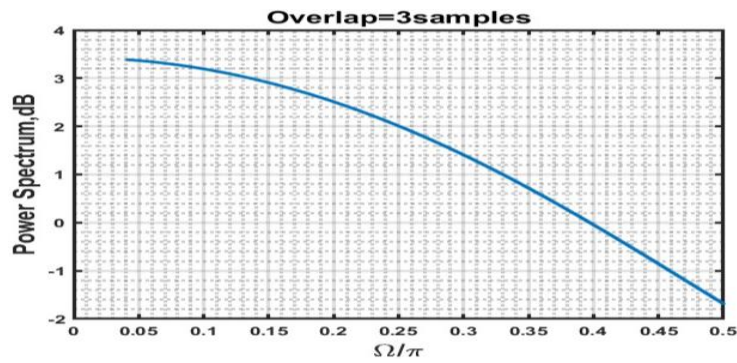
Figure 3. Power Spectrum Graph for the Transmitted

Signals of OFDM

Figure 3 presents a graphical illustration of the power spectral density characteristics inherent in the transmitted signal with an oversampling factor of 4 concerning the number of sub-channels. In the context of OFDM, the CP duration is configured to be 1/4 of the symbol duration. As the number of sub-channels rises, there is an increase in PAPR.
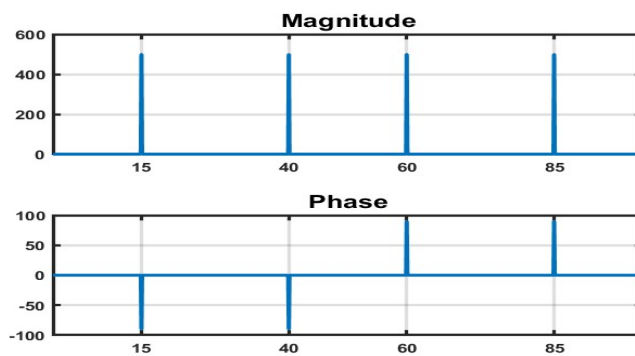
Figure 4. Performance Results for Frequency Response

Figure 4 illustrates the frequency feedback, capturing both magnitude and phase, and the time impulse feedback of two filters: Armstrong's filter (H) and enhanced filter ($H1$, crafted in the initial iteration).
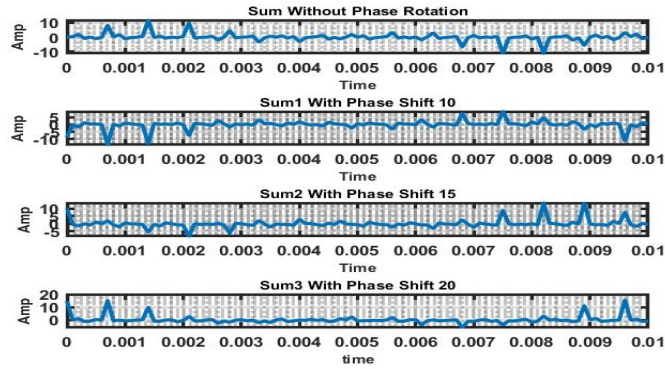
Figure. 5. Numerical Simulation Results for Amplitude with

Different Phase Shifts

Figure 5 displays the numerical simulation results for amplitude under various phase shifts, emphasizing the significance of phase shift information in target detection, particularly on uneven surfaces. The amplitude results are shown for the following scenarios: no phase rotation, phase shift of 10, phase shift of 15, and phase shift of 20. The observations suggest that, based on the simplified model employed, the amplitude of reflection remains unaffected by the surface shape and target features.
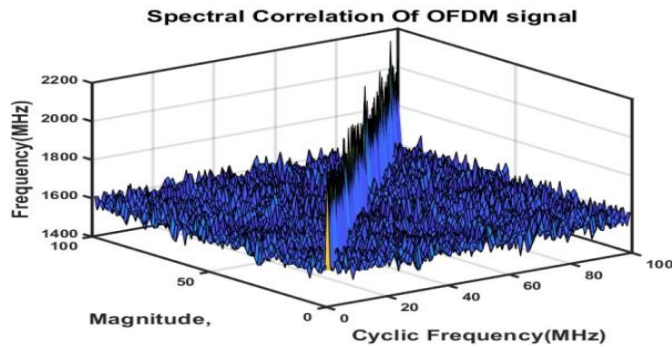
Figure. 6. Spectral Correlation of OFDM Signal

In Figure 6, the illustration portrays the spectral association function of a 5-symbol averaged OFDM signal with pilot subcarriers advanced by 2.5 dB. An OFDM signal recognition scheme is employed, capitalizing on the consistent spacing between successive pilot subcarriers and leveraging the cyclic characteristic of these pilot subcarriers. The figure distinctly reveals the impact of the boosted pilot subcarriers.
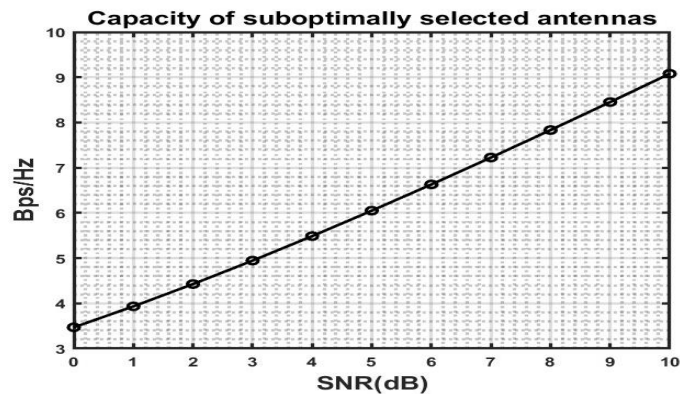
Figure.7. Capacity vs Avg SNR

In Figure 7, the graph showcases the capacity (in bps/Hz) plotted against the avg SNR of MIMO-CDMA in a six-path conduit with incorporated channel approximation. The SNR is precisely well-defined as the power ratio of the entire received signal, encompassing data, pilot, and control signals, to the AWGN.
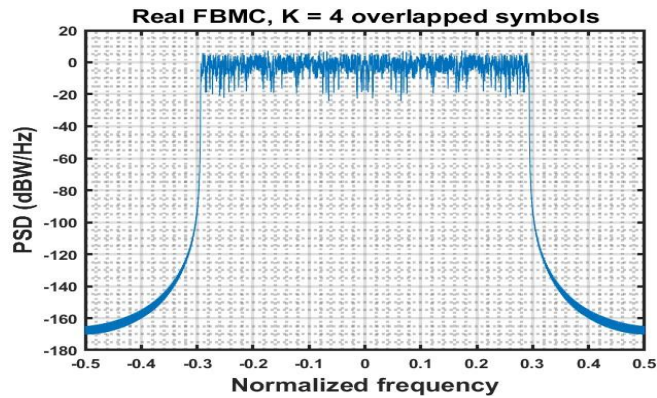
Figure. 8. Power Spectral Density Analysis of FBMC

Figure 8 reveals a notable observation: the spectral concentration of enhanced F-OFDM exhibits inferior side lobes when compared to OFDM. This characteristic unswervingly contributes to a more efficient utilization of the assigned spectrum, resulting in an improved spectral efficiency compared to the existing OFDM system. To further quantify the performance, the individual PAPR for both OFDM and augmented F-OFDM are figured as 9.3401 dB & 10.4366 dB, correspondingly, at a SNR of 20 dB. Additionally, the BER for F-OFDM is calculated to be 0.41546.
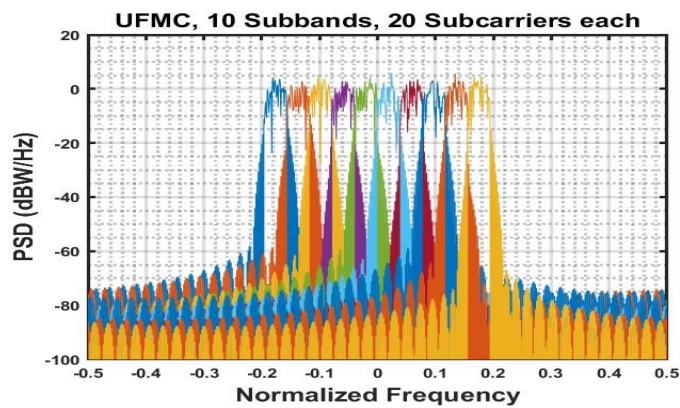
Figure. 9. OFDM & F-OFDM PSD for Filter Orders

Figure 9 provides a visual exposition of the frequency feedback exhibited by the meticulously crafted sieves for Filtered-OFDM (F-OFDM), characterized by NPRB = 6, Ne = 3, and sieve orders of 32, 64, and 128, correspondingly. As observed   above Red-dashed lines elegantly signify the 4 dB cut-off frequency of these filters, strategically positioned at half of the beneficial bandwidth coupled with the surplus bandwidth.
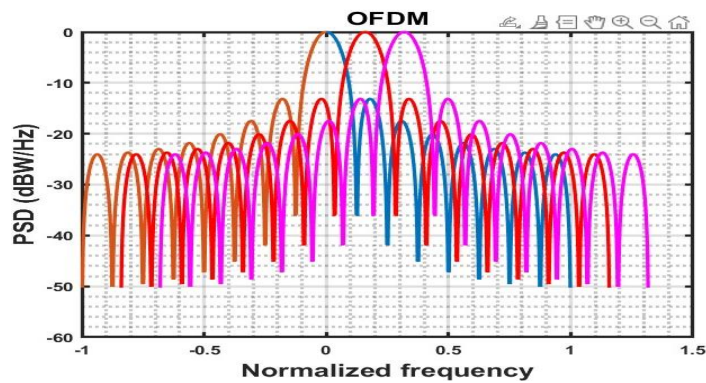
Figure. 10. Contrasting the PSD of F-OFDM with the PSDs

of UFMC and OFDM.

In the illustrious tableau of Figure 10, an extravagant spectacle unfolds as it orchestrates a symphony of

comparison, portraying the majestic execution of the F-OFDM system in regal contrast with the venerable standard OFDM and the distinguished UFMC schemes. This opulent display spotlights the PSD of F-OFDM signal, where the discerning eye is enraptured by the resplendent revelation that F-OFDM graciously bestows upon the observer.
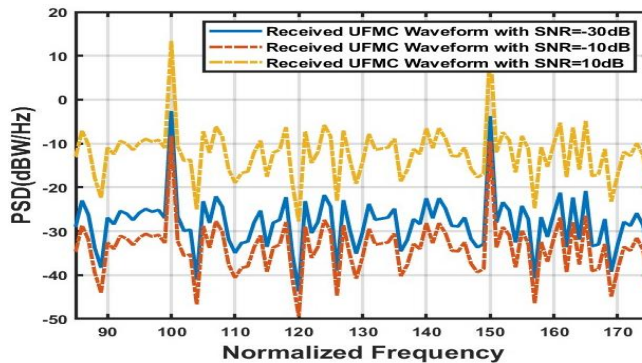
Figure. 11. PSD Estimation of acquired UFMC for

Several SNR rates.

In the captivating visual tapestry of Figure 11, a vivid portrayal unfolds, showcasing the PSDs of the acquired UFMC waveform under the enchanting spell of varying Signal-to-Noise Ratios (SNRs) at distinct decibel levels: (10) dB, (-10) dB, and (-30) dB. Within this mesmerizing spectacle, the amalgamation of noise variance with the gracefully generated waveforms unveils its symphony, reaching its crescendo at the highest noise variance, gracefully embodied by the (-30) dB SNR, and whispering its serenade to the lowest noise variance at the 10 dB SNR. As the diagram gracefully illustrates, the dance of higher noise variance elegantly orchestrates a

higher PSD for the acquired UFMC signal. sonnet.
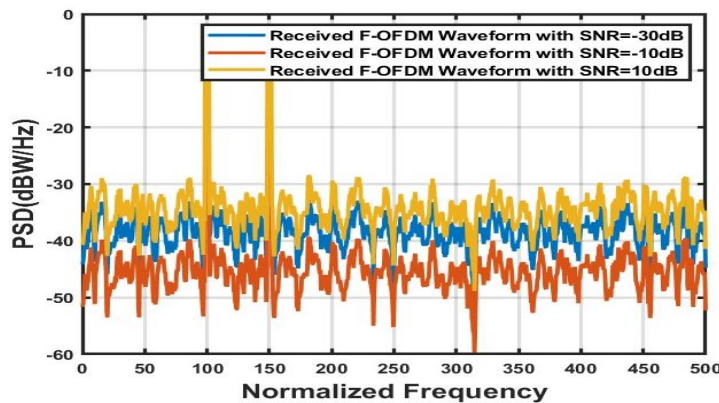
Figure. 12. PSD of Acquired F-OFDM for Several SNR

Rates

Figure 12 displays the PSDs of received F-OFDM signals at different SNRs: -30 dB, -10 dB, and 10 dB. The noise variance sundry through the output signals is most prominent at -30 dB SNR, while 10 dB SNR exhibits the least noise variance. As depicted, higher noise variance directly influences the PSD of the acquired F-OFDM waveform. Subsequently, the F-OFDM signal at 10 dB SNR appears cleaner equated to those at -10 dB and -30 dB SNR values.

Table .1. Performance Values for Proposed Work

Sr. No.	Parameters	Values]
1	Power Spectrum (dB)	-1.63
2	Capacity (Bps/Hz)	9.5
3	Magnitude Response	520
4	PSD (dBW/Hz)	4.5

Table 1 summarizes the performance metrics for the proposed work, providing values for power spectrum, capacity, magnitude response, and PSD. The proposed work yields a power spectrum value of -1.63 dB, a capacity of 9.5 Bps/Hz, a magnitude response of 520, and PSD values of 4.5 dBW/Hz, respectively.
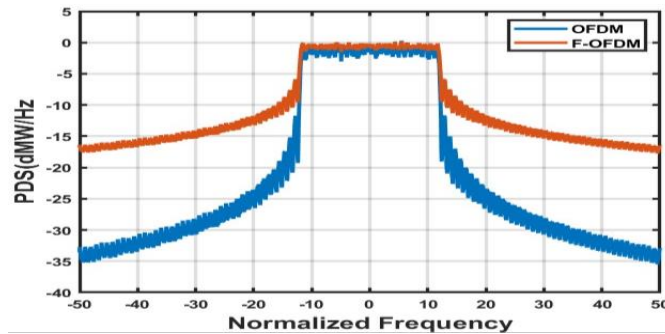
Figure. 13. PSDs Analysis of OFDM & F-OFDMWaveforms

Depiction in figure 13 displays PSD for both OFDM as well as F-OFDM waveforms. In   this comparison, the OOBE (out of band emission) power of standard OFDM is measured at -47 dB, whereas the F-OFDM waveform achieves an impressive -185 dB for OOBE power. These results illustrate a remarkable enhancement in frequency localization for F-OFDM, surpassing OFDM by mitigating OOBE by roughly 138 Db.
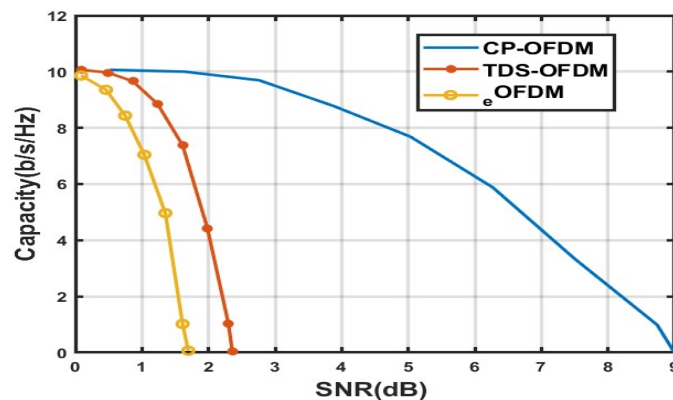
Figure .14. Capacity Performance of Notches Frequency

In the captivating tableau of Figure 14, a visual symphony unfolds, delineating the mean capacity presentation per OFDM subcarrier. This opulent display unveils the performance dynamics within conventional settings, encompassing both 1-tap and 2-tap conduit circumstances, as well as the pre-coded OFDM setups, juxtaposed against the pristine canvas of the original unadorned OFDM setup.
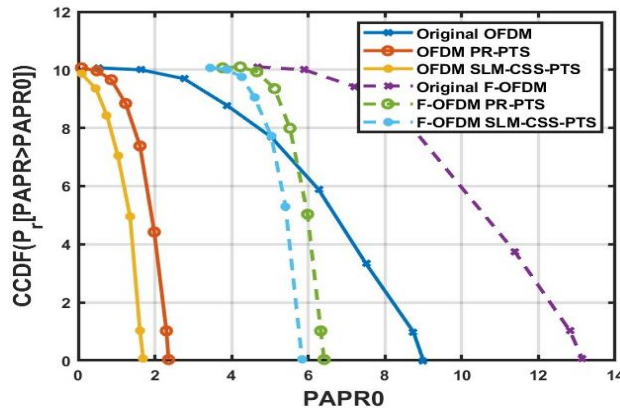
Figure 15. Contrast of PAPR between OFDM & F- OFDM, with N=512 and M=64.

In the illustrative canvas of Figure 15, a compelling portrayal unfolds, delineating the efficacy of PAPR mitigation across diverse setups. Within the realm of OFDM-based systems, the PAPR values stand at 8.73 dB for SLM-CSS-PTS, 9 dB for PR-PTS, and 11.87 dB for the pristine OFDM genesis. Conversely, the F-OFDM realm unveils PAPR values of 10.49 dB for SLM-CSS-PTS, 10.75 dB for PR-PTS, and 13.61 dB for the original F-OFDM masterpiece.
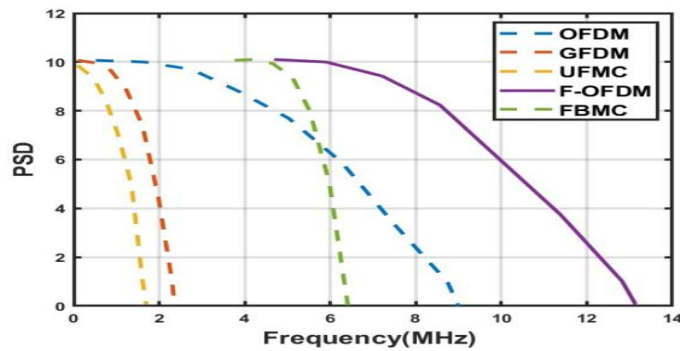
Figure. 16. Power Spectral Density Plot

In figure 16, the PSD computation reveals that OOBE of OFDM sidebands is significantly higher compared to UFMC and FBMC-OQAM. Consequently, the introduced ISI and ICI during symbol transmission are also elevated for OFDM. As a result, the side-lobe attenuation of FBMC is notably higher than UFMC and OFDM. Additionally, the spectral efficiency of FBMC is superior compared to UFMC, while it is considerably lower for CP-OFDM.
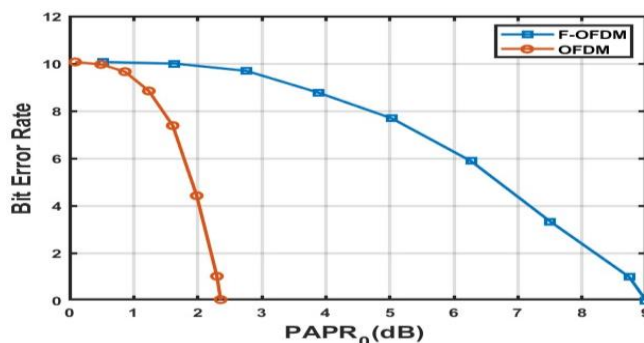
Figure. 17. **64-QAM BER comparison between OFDM &**

F-OFDM**.**

Figure 17. illustrates curves depicting the association among the BER of the OFDM setup and F-OFDM waveform. Here, in this scenario, the AWGN conduit is employed, the constellation plotting for both contexts is set to 64-QAM, whereas the amount of subcarriers is secured at 512. The BER of F-OFDM is nearly equivalent to

OFDM at low-slung values of SNR. However, the BER performance of F-OFDM is slightly advanced than that of OFDM at higher ideals of SNR.
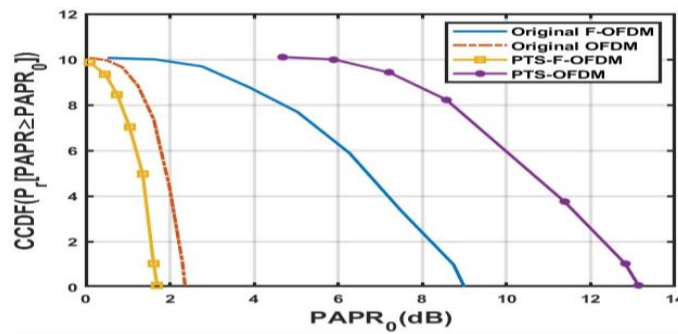
Figure. 18. PAPR evaluation among OFDM & F-OFDM.

Figure 18 illustrates the PAPR efficacy of both OFDM and F-OFDM waveforms with N = 512. In contrast to OFDM, F-OFDM showcases an escalation in PAPR by 1.42 dB devoid of PTS and by 1.73 dB under the absence of PTS. These findings disclose that the PAPR of the F-OFDM waveform outstrips that of the OFDM benchmark by roughly 1.5 dB. This distinction is ascribed to the filter length inherent in the F-OFDM waveform, inducing the mean power of the signal to descend below that of the OFDM reference.
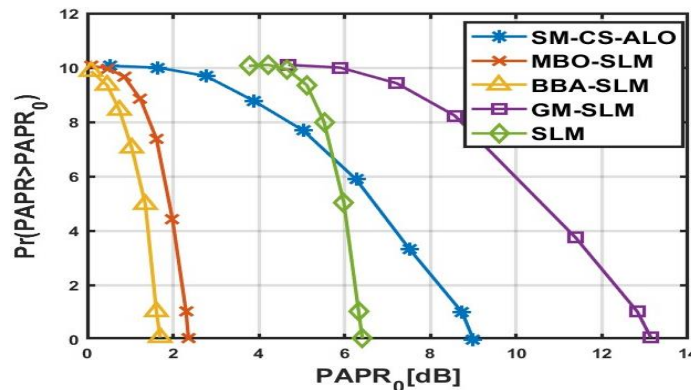
Figure. 19. Comparison Analysis of PAPR with

Existing Techniques.

Figure 19 meticulously scrutinizes the influence of modulation setups on the $PAPR_0$ (dB) -Pr (PAPR > $PAPR_0$) arcs within the realm of the illustrious SM-OHOCO algo, adorned with the presence of the regal 4-QAM modulation setups. This visual masterpiece distinctly unravels that the progenitor prototypical has faltered in attaining a triumphant output, paling in comparison to its Counterparts. Concurrently, the MBO-SLM prototypical emerges as the protagonist, showcasing a substantially elevated performance compared to the original iteration, albeit not eclipsing the prowess of the other distinguished tactics.

Table 2: Comparison Table for PAPR

Sr. No.	Technique	PAPR [dB]
1	MBO-SLM	2.4
2	BBA-SLM	1.7
3	GM-SLM	13.1
4	SLM	6.4
5	SM-CS-ALO (Proposed)	9

Table 3 unveils the PAPR values, orchestrating a symphony of comparison between the heralded introduced methodology and its esteemed counterparts—MBO-SLM, BBA-SLM, and SLM. In this tableau of excellence, the proposed method stands adorned with a regal PAPR value of 9 dB, a testament to its superior performance in comparison to the existing methods. With resounding success, it elegantly diminishes the PAPR, standing head

and shoulders above its counterparts.

VIII. CONCLUSION

FBMC develops as a viable modulation technology for mMIMO channels in future fifth-generation wireless networks. This multi-carrier modulation system, with a wide dynamic range, uses the FBMC modulation algorithm. Unlike classic OFDM, which uses guard intervals such as CP and Known Symbol Padding (KSP) for block construction, this study presents a new technique. The study recommends selecting the guard interval using data symbols and adaptive window-based resilient subcarriers within the block. The study tries to improve the system's BER performance by utilising the high autocorrelation of the chosen guard sequence.

Additionally, the investigation delves into the integration of F-OFDM with the FBMC framework, aiming at PAPR reduction. This is achieved through the implementation of SLM in conjunction with the Cuckoo Search and Ant Lion Optimization (CS-ALO) algorithm. The methodology includes a successive suboptimal cross-antenna rotation scheme, coupled with the generation of FBMC waveforms utilizing DFT augmentation. The proposed approach strives to optimize the performance of the

Experimental results show that the proposed technique significantly improves PAPR reduction compared to conventional methods such as conventional GFDM and OFDM-SLM. The novel scheme is particularly effective for applications involving QAM, providing superior PAPR reduction performance with lower computational complexity.

REFERENCES

[1] Algriree, W., Sulaiman, N., Isa, M., Sahbudin, R.K., Hassan, S.L., Salman, E.H. and Alghrairi, M.,"An analysis of low complexity of 5G-MIMO communication system based CR using hybrid filter detection", Alexandria Engineering Journal, vol. 65, no. 15, 2023, pp. 627-648.

[2] Liu, M., Xue, W., Xu, Y. and Makarov, S.B., "Design of filters based on generic function model for reducing out-of-band emissions of the F-OFDM systems". International Journal of Electronics and Communications, vol. 139, , 2021., pp.153908

[3] Zhang, D. Le Ruyet, D. Roviras, Y. Medjandi & H.Sun. "Spectral efficiency comparison of OFDM/FBMC for uplink cognitive radio networks", EURASIP Journal on Advances inSignal Processing, vol. 1, 2010, pp.1-14.

[4] R. Zhang and C. K. Ho. "MIMO broadcasting for simultaneous wireless information and power transfer," IEEE Trans. Wireless Commun., vol. 12, no. 5, 2013, pp. 1989–2001.

[5] Z. Xiang and M. Tao. "Robust beamforming for wireless information and power Transmission," IEEE Wireless Commun.Lett, vol. 1, no. 4, 2012, pp. 372–375,

[6] B.P. Lathi, Zhi Ding & Hari Mohan Gupta. "Modern digital and analog communication systems," 4th Edition, Oxford University press, 2017.

[7] Ahmad R.S. Bahai, Burton R. Saltzberg and M. Ergen. "Multi-carrier digital communications: theory and applications of OFDM," 2nd Edition, **Springer**, 1999.

[8] A. Shukla and M. Patidar, "BER Analysis of Modulation techniques based OFDM system," International Journal of Innovative Research in Science and Engineering, vol 5, no. 3, 2017, pp.35-41.

[9] S. Hare and R. Prasad. "Multicarrier Techniques for 4G Mobile Communications," Artech House universal personal communications series, 2023.

[10] Dang Shuping et al. "Relay assisted OFDM with subcarrier number modulation in multi-hop cooperative networks", IEEE Wireless Communications Letters, vol. 9, no. 11, 2020. pp. 1869-1873,

[11] X. Zhou, R. Zhang, and C. K. Ho. "Wireless information and power transfer: architecture design and rate-energy trade-off," IEEE Trans. Commun., vol. 61, no. 11, 2013, pp. 4754–4767.

[12] L. Liu, R. Zhang, and K. C. Chua. "Wireless information and power trasfer: a dynamic power splitting approach," IEEE Trans. Commun., vol. 61, no. 9, 2013, pp. 3990–4001.

[13] J. Pak and B. Clerckx "Joint wireless information and energy transfer in a two-user MIMO interference channel," IEEE Trans.Wireless Commun., vol. 12, no. 8, 2013, pp. 4210–4221.

[14] A. Nasir, X. Zhou, S. Durrani, and R. A. Kennedy. "Relaying protocols for wireless energy harvesting and information processing," IEEE Trans. Wireless Commun., vol. 12, no.7, 2013.pp, 3622–3636.

[15] A. Shivhare, M. Patidar and R. Kumar. "Review of MIMO-OFDM System Using Simulink Model", International Journal of Computer Sciences and Engineering, vol.7, no.3, pp. 72-75, 2019.

[16] Satish Kumar and K. R. Shankar Kumar, "Adaptive genetic based watr filling approach for power & bit allocation in MIMO OFDM system," Journal of Theoretical and AppliedInformation Technology, vol. 63, no. 2, 2014, pp. 396-407.

[17] Unnisa, N. and Tatineni, M. "Adaptive deep learning strategy with red deer algorithm for sparse channel estimation and

hybrid precoding in millimeter wave massive MIMO-OFDM systems", Wireless Personal Communications, vol. 122, no. 4,2022, pp.3019-3051.

[18] Hu, F., Xu, H., Jin, L., Liu, J., Xia, Z., Zhang, G. and Xiao,J."Continuous-unconstrained and global optimization for PSO-PTS based PAPR reduction of OFDM signals. Physical Communication", vol.55, 2022, pp.101825.

[19] H. Zhang, D. Le Ruyet, D. Roviras, Y. Medjandi and H. Sun, "Spectral Efficiency Comparison of OFDM/FBMC for Uplink Cognitive Radio Networks", EURASIP Journal on Advances in Signal Processing, vol. 1, 2010, pp. 1-10.

[20] Z. Xiang and M. Tao. "Robust beamforming for wireless information and power Transmission," IEEE Wireless Commun.Lett, vol. 1, no. 4, 2012, pp. 372–375.

[21] Vieira, L.C., Ozan, W., Mitchell, J. and Darwazeh, I.,J. "Modeling and compensation of nonlinear distortion in direct-detection optical Fast-OFDM systems". 13th International Symposium on Communication Systems, Networks and Digital Signal Processing (CSNDSP), july 2022, pp. 168-173.

[22] Hu, F., Xu, H., Jin, L., Liu, J., Xia, Z., Zhang, G. and Xiao, J. "Continuous-unconstrained and global optimization for PSO-PTS based PAPR reduction of OFDM signals". Physical Communication, 55, p.101825, 2022.

[23] Haijian Zhang, "Spectral Efficiency Analysis in OFDM and OFDM/OQAM based Cognitive Radio Networks", IEEE Vehicular Technology Conference, 2009.

[24] J. Xu, L. Liu and R. Zhang., "Multiuser MISO beamforming for simultaneous wireless Information and power transfer", Proc. IEEE Int.onf. Acoust. Speech Signal Process.pp. 1-17,2013.

[25] Manoj Kumar, Manish Patidar and Narendra Singh. "Analysis of OFDMA over different channel", International Conference on Cognitive & Intelligent Computing. vol.2,pp.1-6, 2021.

[26] Manoj Kumar, Manish Patidar and Narendra Singh. "Optimized MIMO based enhanced W-OFDM for Multi-carrier communication system with 5G waveform", ECECSR Journal, vol.57, no. 2, 2023,pp. 1-24.

[27] Vaigandla, K.K. and Benita, J., "Novel Algorithm for Nonlinear Distortion Reduction Based on Clipping and Compressive Sensing in OFDM/OQAM System". IJEER, vol.10, no.3, 2021,pp-620-626.

[28]   S. Rangaraju, "AI Sentry: Reinventing Cybersecurity Through Intelligent Threat Detection," EPH - International Journal of Science and Engineering, vol. 9, no. 3, pp. 30–35, Dec. 2023. DOI: [10.53555/ephijse.v9i3.211](https://doi.org/10.53555/ephijse.v9i3.211).

[29] Md. Touhidul Islam, Md. Muaz Hussain, Md. Saneul Alam Shiam, Minhazul Abedin, and Md. Erfanul Hoque, "Land Use and Land Cover Change And Its Effect On Land Surface Temperature: An Impact Analysis Of Rohingya Influx In Ukhia Upazila Between Year 2000 To 2020," EPH - International Journal of Science And Engineering (ISSN: 2454 - 2016), vol. 9, no. 3, pp. 77–96, Dec. 2023. DOI: [10.53555/ephijse.v9i3.222](https://doi.org/10.53555/ephijse.v9i3.222)

[30] S. Zhuo, Y. Y. Hong, and T. D. Palaoag, "An Intelligent Cyber Security Detection and Response Platform," International Journal for Research in Advanced Computer Science and Engineering, vol. 8, no. 12, pp. 1–10, Dec. 2022. DOI: [10.53555/cse.v8i12.2167](https://doi.org/10.53555/cse.v8i12.2167)